

FLOW STRESS BEHAVIOR AND GOVERNING EQUATION OF PLASTIC FLOW OF LOW-CARBON STEEL AT ELEVATED TEMPERATURES

Z. Y. Wang,¹ M. X. Ma,² S. Zhong,³ S. Zhang,³ J. Feng,² H. L. Wu,¹ and Yu. Cao¹

Translated from *Metallovedenie i Termicheskaya Obrabotka Metallov*, No. 6, pp. 42 – 48, June, 2023.

Original article submitted March 17, 2022.

The effect of hot isothermal compression on the flow stress of low-carbon steel was studied using a Gleeble 3500 stimulator at temperatures from 900 to 1200°C and deformation rates from 0.01 to 10 sec⁻¹. The flow stress was analyzed at elevated temperatures using a hyperbolic sine function. The material constants were determined in the range of true deformation rates from 0.1 to 0.7. The dislocation structure of low-carbon steel was studied after the deformation at 1100°C and cooling at a rate of 5 K/sec. A governing equation for describing and simulating the low-carbon steel behavior under high-temperature deformation was derived and justified. It was shown that the obtained equation can be used to provide a reliable and valid description of the low-carbon steel behavior under hot forming with a mean relative error of 5.1219% and a correlation coefficient of 0.9886. The equation can be used to model and optimize the process parameters of hot deformation of steel and to predict the evolution of its microstructure.

Key words: low-carbon steel, hot deformation, evolution of microstructure, governing equation.

INTRODUCTION

Modern low-carbon steels are widely used in automotive, construction, power-generation, transportation, machine-building and other industries. This is due to the ability to achieve a combination of high strength, ductility, and impact toughness of steels, as well as their good formability under elevated temperatures [1, 2]. It is known that the formability of materials in the hot state depends on their controlled process parameters and flow characteristics [3]. Each combination of thermomechanical processing (TMP) parameters leads to a specific deformation behavior, type of structure, and combination of steel properties [4 – 10]. Knowing the deformation behavior (and a corresponding governing equation) of an alloy is of great importance for quantitative analysis of the deformation processes and optimization of the processing technology.

The microstructure of steel formed in the process of deformation depends on its deformation behavior and mechanical characteristics, as well as the TMP parameters, such as stress, deformation rate, temperature, etc. [9]. The deformation behavior of the material can be simulated using a governing equation with an effective mathematical representation based on a limited number of experimental data [11 – 13]. Simulation of material deformation under different loading conditions can be performed using the finite element method [14 – 16] by applying commercially available software. Similar studies of low-carbon steel have been conducted and described in Ref. [11, 17 – 19]. However, these studies are dedicated to analyzing the behavior of steel during hot deformation in the ferrite region, or at low deformation rates. There are significantly fewer studies on hot deformation of low-carbon steel in the austenite region [20 – 22]. Therefore, it is important to study the behavior of low-carbon steel during hot deformation in the austenite region to understand the nature of deformation, establish a governing equation, and optimize the TMP parameters.

The objective of this work is to study the specifics of low-carbon steel behavior during deformation under hot isothermal compression in the temperature range from 900 to 1200°C and deformation rates from 0.01 to 10 sec⁻¹.

¹ School of Mechanical and Material Engineering, Wu Zhou University, Wu Zhou, Guangxi, China (e-mail: zheyang_wang@sina.com).

² School of Mechanical Engineering and Automation, Northeastern University, Shenyang, Liaoning, China (e-mail: mxma@mail.neu.edu.cn).

³ School of Materials Science and Engineering, Shenyang University of Technology, Shenyang, Liaoning, China.

TABLE 1. Parameters of Hot Isothermal Compression

Deformation temperature, °C	Deformation rate, sec ⁻¹	Degree of deformation
1200	0.01	0.1
1100	0.1	0.2
1000	1	0.3
900	10	0.4
		0.5
		0.6
		0.7

METHODS OF STUDY

The chemical composition of the studied steel was determined using atomic emission spectroscopy and includes the following elements, wt.%: C — 0.16; Mn — 0.7; Si — 0.15; Cu — 0.15; S — 0.05; and P — 0.04.

Cylindrical samples measuring 4 mm in diameter and 8 mm in height were cut out from cast blanks with a tolerance of 0.02 mm. The flat ends of the samples were immersed in graphite lubricant to a depth of 0.1 mm in order to minimize friction during hot forming (stamping). Hot isothermal compression experiments were conducted by using a Gleeble 3500 simulator. The process parameters of hot isothermal compression are shown in Table 1.

The samples were heated in a Gleeble 3500 setup at a rate of 10 K/sec using direct resistance heating [21, 23, 24]. After reaching the desired test temperature, the samples were soaked for 4 min to achieve a stable and homogeneous temperature field, after which the deformation started. The temperature was controlled with an accuracy of $\pm 5^\circ\text{C}$ using two type K thermocouples installed in the middle of the sample lengthwise. During each test, after achieving a specified degree of deformation ($\varepsilon = 0.1 - 0.7$), the sample was immediately quenched in water to room temperature to fix the hot-deformed structure of steel.

During compression experiments, the effect of thermo-mechanical process parameters on the flow stress of low-carbon steel was determined. Based on the obtained results, the governing equation of steel flow was derived using regression analysis, which included temperature, deformation rate, and degree of deformation. The apparent activation energy of hot deformation was also calculated, and stress multipliers, stress exponent, and Zener–Hollomon parameters were determined.

EXPERIMENTAL RESULTS

The experimental stress–strain curves for the studied steel obtained during hot isothermal compression at temperatures ranging from 900 to 1200°C and deformation rates ranging from 0.01 to 10 sec⁻¹ are shown in Fig. 1. As can be seen, the behavior of all curves in the initial section is the

same, namely, the stress linearly increases with deformation until reaching its maximum (peak) value at this stage. During this stage of steel deformation, the behavior of the compression curves is independent of temperature and deformation rate. However, these parameters have a significant effect on the stress value. The latter decrease at higher temperatures and lower deformation rates [25]. The peak stress is the lowest at the highest temperature (1200°C) and the lowest deformation rate (0.01 sec⁻¹). After reaching the peak stress, the behavior of all curves changes abruptly: the stress either increases very slowly or remains practically constant with increasing deformation. When deforming steel at a rate of 0.01 sec⁻¹, nearly flat stress–strain curves are observed past the peak stress, which indicates a steady-state flow of the metal. When deforming steel at a rate of $\nu = 0.1 \text{ sec}^{-1}$, the curves demonstrate a slight increase past the peak stress, while in case of $\nu = 1$ and 10 sec⁻¹, deformation hardening develops.

As is well-known, deformation hardening is caused by an increase in the dislocation density in metallic materials, which is the most effective at higher deformation rates. In this case, the interstitial atoms (C and N) in ferrite interact elastically with dislocations, which leads to a further increase in the flow stress [26, 27].

Two characteristic features should be noted in the initial section of the flow stress curves at high deformation rates. One of them is that in the early stage of deformation, the flow stress rapidly increases to a fixed value, since deformation hardening caused by multiplication and interaction of dislocations becomes dominant. In this case, the rate of dynamic softening, caused by dislocation cross-sliding and climb, is lower than the rate of deformation hardening. The second feature has to do with the fact that after reaching the peak stress, a steady-state flow of metal is observed. In other words, a substructure is formed, in which dynamic softening, due to the processes of annihilation of dislocations having opposite signs, balances deformation hardening caused by an increase in dislocation density [28, 29].

The dislocation structure of steel after deformation at 1100°C at a rate of 1 sec⁻¹ with subsequent cooling at a rate of 5 K/sec is shown in Fig. 2. As can be seen, the carbonitride inclusions, precipitated in austenite, mainly have a spherical shape. The formation of carbonitrides in austenite primarily occurs at the boundaries of austenite grains and subgrains, as well as on dislocations. The precipitated carbonitride inclusions effectively pin these structural elements, thus hindering their movement. In this case, the distribution of carbonitrides, nucleated and precipitated on dislocations, is more uniform compared to those formed at the grain and subgrain boundaries. On one hand, such processes can effectively inhibit the coarsening of austenite grains, since the growth rate of carbonitride inclusions on dislocations is lower than at the grain and subgrain boundaries, resulting in smaller inclusion sizes (around 10 nm) and a more uniform distribution. On the other hand, the effect of nucleation and

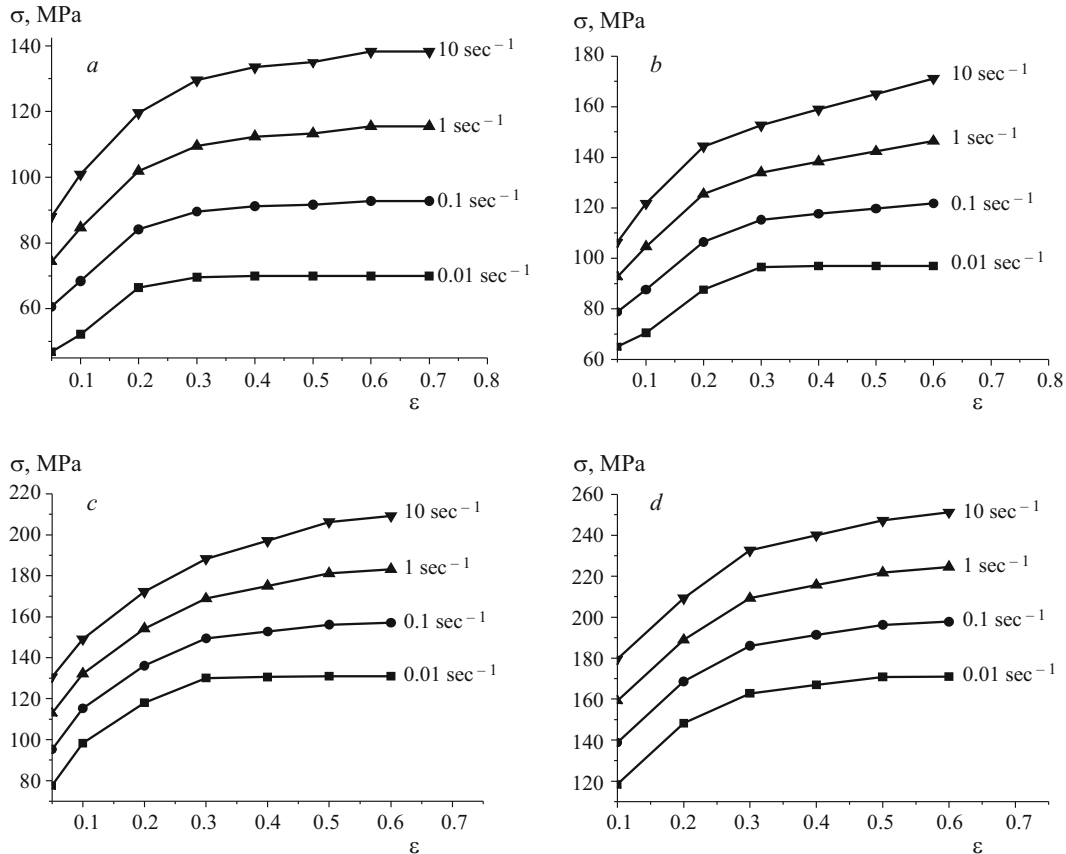


Fig. 1. Stress–strain curves ($\sigma - \epsilon$) of true deformation of low-carbon steel at different deformation rates (see numbers next to the curves) at temperatures of 1200°C (a), 1100°C (b), 1000°C (c), and 900°C (d).

precipitation of carbonitrides near dislocations contributes to an increase in flow stress of the metal past the peak stress as the deformation increases.

The main equation (a mathematical model that describes the deformation behavior of metal) reflects the relationships between the flow stress, deformation rate, and deformation temperature. The governing relationship is not only an important prerequisite for numerical simulation of the metal forming processes, but is also a crucial basis for selecting thermodynamic parameters of deformation and determining technical characteristics of the equipment. The equation can also be used to determine the deformation stability zone according to the dynamic equation of dissipative structure theory. The phenomenological governing equation, which is the most commonly used, can be applied to characterize the dynamic behavior of the material using measurable macro-parameters without considering the microstructure. It can be obtained from the experimental data during thermal simulation of compression, making it convenient for solving various engineering problems.

For the majority of metallic materials subjected to hot deformation, the relationship between the deformation rate and flow stress is formulated using power law (Eq. 1), exponential law (Eq. 2), and hyperbolic sine law (Eq. 3). Equation (1) is typically used in case of low stresses, while Eq. (2)

is used at high stresses. Equation (3), which corresponds to the hyperbolic sine law and was proposed by Sellars and Tegart, is a modified Arrhenius equation that includes the activation energy of plastic deformation (Q) and deformation

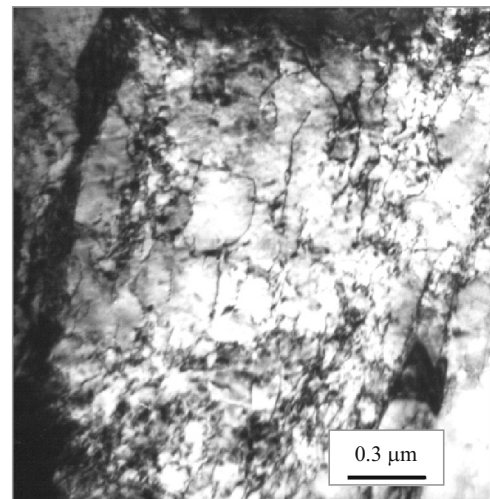


Fig. 2. Dislocation structure of low-carbon steel after deformation at 1100°C at a rate of 1 sec^{-1} followed by cooling at a rate of 5 K/sec.

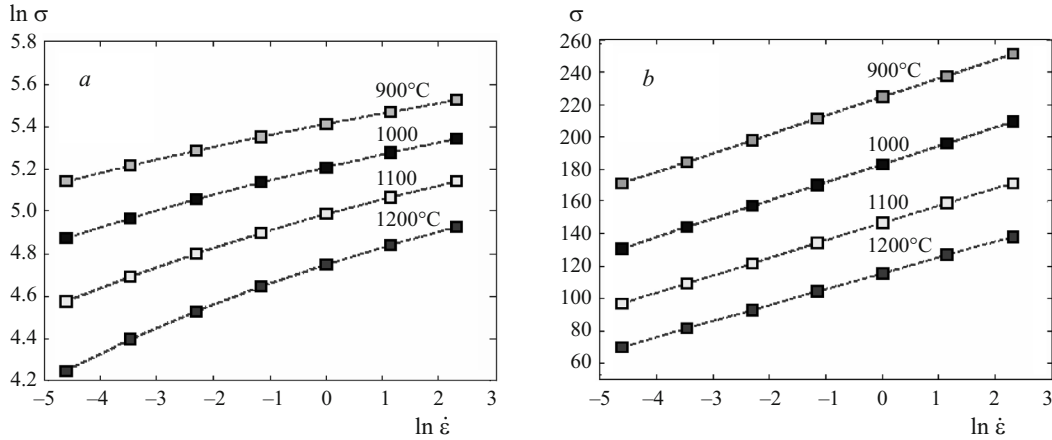


Fig. 3. Relationships $\ln \sigma = f(\ln \dot{\epsilon})$ (a) and $\sigma = f(\ln \dot{\epsilon})$ (b): numbers next to the curves indicate deformation temperatures.

temperature (T). These equations can be used over a wide range of stresses, temperatures, and deformation rates:

$$\dot{\epsilon} = A_1 \sigma^{n_1}, \quad (1)$$

$$\dot{\epsilon} = A_2 \exp(\beta\sigma), \quad (2)$$

$$\dot{\epsilon} = A [\sinh(\alpha\sigma)]^n \exp(-Q/RT), \quad (3)$$

where A_1 , A_2 , A , n_1 , n , β , and α are material constants; σ is the flow stress, MPa; T is the absolute deformation temperature, K; $R = 8.314 \text{ J}/(\text{mol} \cdot \text{K})$ is the universal gas constant; and Q is the deformation activation energy, kJ/mol. In Eq. (3), parameter $\alpha = \beta/n_1$. It has been experimentally confirmed that Eq. (3) can reliably describe the process of conventional hot deformation of metals.

K. Zener and J. G. Hollomon proposed to describe the effect of deformation rate and temperature on the deformation behavior of metals using a Z -parameter, the validity of which was confirmed by them later experimentally. Z -parameter represents a Zener-Hollomon parameter and can be determined from the following equation:

$$Z = \dot{\epsilon} \exp(Q/RT) = A [\sinh(\alpha\sigma)]^n. \quad (4)$$

By taking the natural logarithm of both sides of Eqs. (1), (2), and (3), the following is obtained:

$$\ln \dot{\epsilon} = \ln A_1 + n_1 \ln \sigma, \quad (5)$$

$$\ln \dot{\epsilon} = \ln A_2 + \beta\sigma, \quad (6)$$

$$\ln \dot{\epsilon} = \ln A + n \ln [\sinh(\alpha\sigma)] - Q/RT. \quad (7)$$

After substituting deformation rates ($0.01 - 10 \text{ sec}^{-1}$) and flow stress values at a true degree of deformation ($\epsilon = 0.5$) into Eq. (5), (6), and (7), the $\ln(\dot{\epsilon}) - \ln(\sigma)$ and $\ln(\dot{\epsilon}) - \sigma$ relationships can be obtained for different deforma-

tion temperatures (Fig. 3). By applying linear regression to the $\ln(\dot{\epsilon}) - \ln(\sigma)$ and $\ln(\dot{\epsilon}) - \sigma$ relationships, the slopes of the lines can be determined for deformations at different temperatures. Parallel lines with the same slopes indicate that the $\ln(\dot{\epsilon}) - \ln(\sigma)$ and $\ln(\dot{\epsilon}) - \sigma$ relationships are independent of temperature. By averaging the slopes of the graphs in Fig. 3, the following parameters can be calculated: $n_1 = 13.7404$ and $\beta = 0.0921 \text{ MPa}$. Then, $\alpha = \beta/n_1 = 0.0067 \text{ MPa}$.

By finding particular solutions of the differential equation (7), the following relationships can be obtained:

$$n = \left[\frac{\partial \ln \dot{\epsilon}}{\partial \ln [\sinh(\alpha\sigma)]} \right]_T, \quad (8)$$

$$Q = R \left[\frac{\partial \ln \dot{\epsilon}}{\partial \ln [\sinh(\alpha\sigma)]} \right]_T \left[\frac{\partial \ln [\sinh(\alpha\sigma)]}{\partial (1/T)} \right]_{\dot{\epsilon}}. \quad (9)$$

The values of deformation rate and true stresses for a true deformation ($\epsilon = 0.5$) can be substituted into Eq. (8). The resulting relationship $\ln(\dot{\epsilon}) - \ln [\sinh(\alpha\sigma)]$ for different deformation temperatures is graphically shown in Fig. 4a. Parameter n , calculated as the average slope of these curves, is equal to 10.1352. The $\ln [\sinh(\alpha\sigma)] - 1/T$ relationship at different deformation rates can be obtained by substituting experimental parameters into Eq. (9), as shown in Fig. 4b. The curves shown in Fig. 4b were used to calculate the average level of activation energy $Q = 207.613 \text{ kJ}/\text{mol}$ for a true deformation ($\epsilon = 0.5$). The following thermodynamic parameters were obtained for low-carbon steel during hot compression: $\alpha = 0.0067 \text{ MPa}^{-1}$; $n = 10.1352$; $A = 2.131 \times 10^9 \text{ sec}^{-1}$; $Q = 207.613 \text{ kJ}/\text{mol}$.

Taking the logarithm of both sides of Eq. (4) results in the following relationship:

$$\ln Z = \ln A + n \ln [\sinh(\alpha\sigma)]. \quad (10)$$

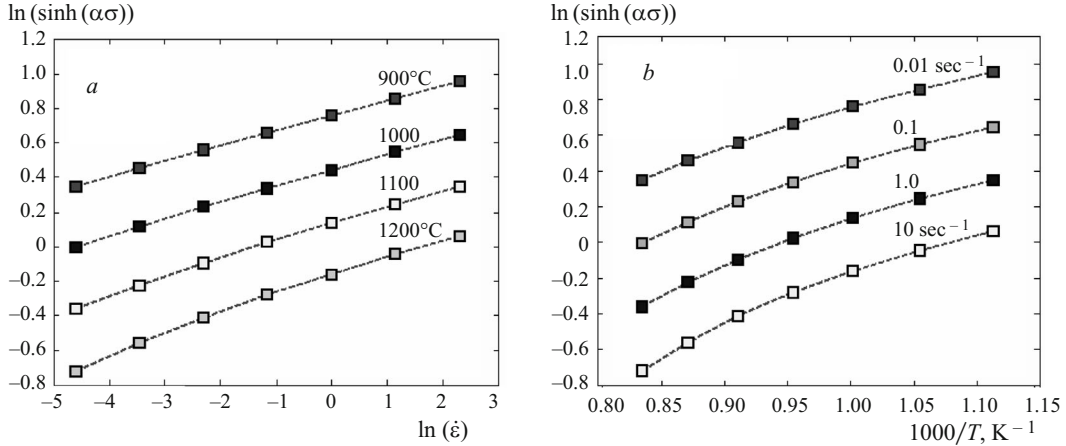


Fig. 4. Relationships $\ln [\sinh (\alpha \sigma)]=f(\ln \dot{\epsilon})$ (a) and $\ln [\sinh (\alpha \sigma)]=f(1000 / T)$ (b) for low-carbon steel at a true deformation ($\epsilon = 0.5$). Numbers next to the curves: a) deformation temperature; b) deformation rate.

By substituting parameters α and Q into Eq. (10), relationship $\ln Z - \ln [\sinh (\alpha \sigma)]$ can be obtained for a true deformation ($\epsilon = 0.5$) (Fig. 5). By using linear regression, it becomes possible to calculate the intersection point of the obtained curve. The calculated value of $\ln A$ is 21.4797, then $A = 2.131 \times 10^9$; $n = 10.1352$; and $Q = 207.613$ kJ/mol. Therefore, the governing equation for the plastic flow of low-carbon steel at elevated temperatures is expressed by the following three equations:

$$\sigma = \frac{1}{\alpha} \ln \left\{ \left(\frac{Z}{A} \right)^{1/n} + \left[\left(\frac{Z}{A} \right)^{2/n} + 1 \right]^{1/2} \right\}; \quad (11)$$

$$\sigma = \frac{1}{0.0067} \times \ln \left\{ \left(\frac{Z}{2.131 \times 10^9} \right)^{\frac{1}{10.1352}} + \left[\left(\frac{Z}{2.131 \times 10^9} \right)^{\frac{2}{10.1352}} + 1 \right]^{\frac{1}{2}} \right\}; \quad (12)$$

$$Z = \dot{\epsilon} \exp \left(\frac{2.131 \times 10^9}{RT} \right). \quad (13)$$

To assess the adequacy of the derived governing equation for the plastic flow of steel, we will calculate the flow stress values at temperatures ranging from 900 to 1200°C and deformation rates ranging from 0.01 to 10 sec^{-1} at $\epsilon = 0.5$ using Eqs. (11) – (13). The comparison between the experimental stress values and those calculated by using the governing equation is shown in Fig. 6. The correlation coefficient (R) and the average absolute relative error ($AARE$) were evaluated using the following equations:

$$R = \frac{\sum_{i=1}^N (\sigma_e^i - \bar{\sigma}_e)(\sigma_c^i - \bar{\sigma}_c)}{\sqrt{\sum_{i=1}^N (\sigma_e^i - \bar{\sigma}_e)^2 (\sigma_c^i - \bar{\sigma}_c)^2}}; \quad (14)$$

$$AARE = \frac{1}{N} \sum_{i=1}^N \left| \frac{\sigma_e^i - \sigma_c^i}{\sigma_e^i} \right|, \quad (15)$$

where N is the total number of data points; σ_e and σ_c are the experimental and calculated stress values, respectively; and $\bar{\sigma}_e$ and $\bar{\sigma}_c$ are their respective mean values [13]. Based on the data shown in Fig. 6, the following value of the coefficient of correlation between the experimental and calculated data was determined: $R = 0.9886$, while the $AARE$ value was only 5.1219%. This indicates the adequacy and reliability of the obtained hyperbolic sinusoidal function of the Z -parameter

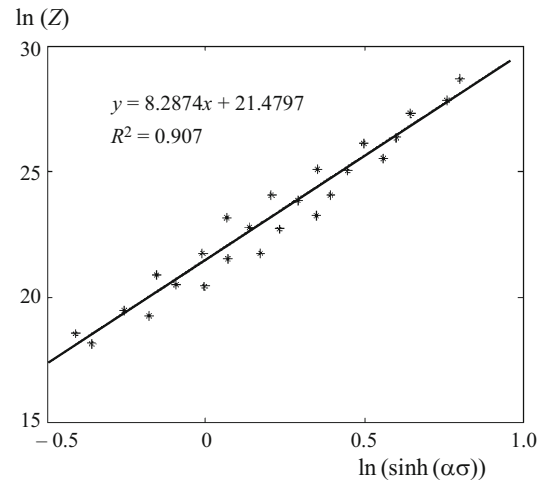


Fig. 5. Graphical representation of the relationship $\ln (Z)=f(\ln [\sinh (\alpha \sigma)])$.

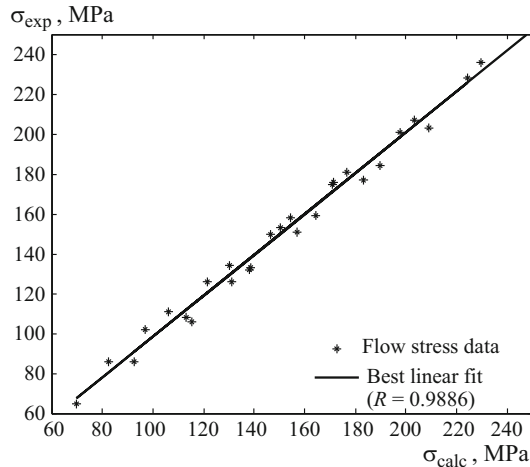


Fig. 6. Correlation between experimental and calculated values of the flow stress of low-carbon steel at various temperatures (calculations were performed using the defining equation): symbols — flow stress values; line — best linear fit ($R = 0.9886$).

for calculating the flow stress of low-carbon steel under high-temperature deformation conditions.

CONCLUSIONS

1. The deformation behavior of low-carbon steel during hot isothermal compression at temperatures from 900 to 1200°C and deformation rates from 0.01 to 10 sec⁻¹ was studied.

2. The flow stress during isothermal compression of low-carbon steel significantly depends on the deformation rate and temperature. The nature of the obtained flow curves of the metal demonstrate the typical dynamic competition between deformation hardening and softening due to dynamic recovery.

3. The flow stress of steel decreases at higher temperatures and lower deformation rates. These dependencies can be described by the governing equation utilizing the Zener–Hollomon parameter (Z). A governing equation for hot isothermal deformation of low-carbon steel was derived as a function of deformation temperature, deformation rate, and calculated material parameters (α , n , and A). The calculated value of the activation energy for deformation is $Q = 207.613$ kJ/mol.

4. The statistical assessment of reliability of the derived governing equation for the plastic flow of steel showed that the average relative error of calculating the flow stress of steel was 5.1219%, and the correlation coefficient was 0.9886. This indicates that the derived governing equation offers a satisfactory description of the behavior of low-carbon steel during hot deformation.

The authors gratefully acknowledge to the financial support for this research from National Key Research and Development Program of China (No. 2019YFB1705002),

Wuzhou University Research Foundation for Advanced Talents (No. WZUQDJJ30056) and Wuzhou Science, Technology Funded Project (No. 202002014) and Doctoral Fund Project of Wuzhou University (2021A003).

REFERENCES

1. R. Jie, Y. X. Xu, J. X. Liu, et al., “Effect of strength and ductility on anti-penetration performance of low-carbon alloy steel against blunt-nosed cylindrical projectiles,” *Mater. Sci. Eng. A*, **682**, 312 – 322 (2017).
2. B. Eric, B. Régis, R. Sophie, and F. Pierre, “Experimental investigation of the thixoforging of tubes of low-carbon steel,” *J. Mater. Process. Tech.*, **252**, 485 – 497 (2018).
3. X. Li, T. F. Jing, M. M. Lu, and J. W. Zhang, “Microstructure and mechanical properties of ultrafine lath-shaped low carbon steel,” *J. Mater. Eng. Perform.*, **21**, 1496 – 1499 (2012).
4. T. Nipon, C. M. Kan, and S. Chao, “Effects of carbon and nitrogen on the microstructure and mechanical properties of carbonitrided low-carbon steel,” *J. Mater. Eng. Perform.*, **24**, 4853 – 4862 (2015).
5. S. Vasanth, M. Bilal, A. Georges, and H. Ramsey, “Friction stir welding of low-carbon AISI 1006 steel: room and high-temperature mechanical properties,” *J. Mater. Eng. Perform.*, **27**, 1673 – 1684 (2018).
6. S. Paul, U. Ahmed, and G. Megahed, “Effect of hot rolling process on microstructure and properties of low-carbon al-killed steels produced through TSCR technology,” *J. Mater. Eng. Perform.*, **20**, 1163 – 1170 (2011).
7. A. Deva, B. K. Jha, and N. S. Mishra, “Influence of boron on strain hardening behaviour and ductility of low carbon hot rolled steel,” *Mater. Sci. Eng. A*, **528**, 7375 – 7380 (2011).
8. M. J. Kang, J. Y. Park, S. S. Sohn, et al., “Interpretation of quasi-static and dynamic tensile behavior by digital image correlation technique in Twinning Induced Plasticity (TWIP) and low-carbon steel sheets,” *Mater. Sci. Eng. A*, **693**, 170 – 177 (2017).
9. J. Hu, L. X. Du, J. J. Wang, et al., “Structure-mechanical property relationship in low carbon microalloyed steel plate processed using controlled rolling and two-stage continuous cooling,” *Mater. Sci. Eng. A*, **585**, 197 – 204 (2013).
10. X. Li, T. F. Jing, M. M. Lu, et al., “Property of nano-grained delaminated low-carbon steel sheet,” *J. Mater. Process. Tech.*, **27**, 364 – 368 (2011).
11. X. W. Yang and W. Y. Li, “Flow behavior and processing maps of a low-carbon steel during hot deformation,” *Metall. Mater. Trans. A*, **46**(12), 6052 – 6064 (2015).
12. J. H. Kim, S. K. Kim, C. S. Lee, et al., “A constitutive equation for predicting the material nonlinear behavior of AISI 316L, 321, and 347 stainless steel under low-temperature conditions,” *Int. J. Mech. Sci.*, **87**, 218 – 225 (2014).
13. X. J. Gao, Z. Y. Jiang, D. B. Wei, et al., “Constitutive analysis for hot deformation behavior of novel bimetal consisting of pearlitic steel and low carbon steel,” *Mater. Sci. Eng. A*, **595**, 1 – 9 (2014).
14. B. Vadavadagi, S. Shekhawat, I. Samajdar, and K. Narasimhan, “Forming limit curves in low-carbon steels: improved prediction by incorporating microstructural evolution,” *Int. J. Adv. Manuf. Tech.*, **86**, 1027 – 1036 (2016).
15. S. Siamak, “Modelling the warm rolling of a low carbon steel,” *Mater. Sci. Eng. A*, **371**, 318 – 323 (2004).

16. Y. Sun, K. Maciejewski, and H. Ghonem, "Simulation of viscoplastic deformation of low carbon steel structures at elevated temperatures," *J. Mater. Eng. Perform.*, **21**, 1151 – 1159 (2012).
17. V. I. Gorynin, S. Yu. Kondratyev, and M. I. Olenin, "Raising the resistance of pearlitic and martensitic steels to brittle fracture under thermal action on the morphology of the carbide phase," *Met. Sci. Heat Treat.*, **55**, 9 – 10, 533 – 539 (2014).
18. J. Wang, H. Xiao, H. B. Xie, et al., "Study on hot deformation behavior of carbon structural steel with flow stress," *Mater. Sci. Eng. A*, **539**, 294 – 300 (2012).
19. J. H. Chung, J. K. Park, T. H. Kim, et al., "Study of deformation-induced phase transformation in plain low carbon steel at low strain rate," *Mater. Sci. Eng. A*, **527**(20), 5072 – 5077 (2010).
20. Y. C. Lin, M. S. Chen, and J. Zhong, "Numerical simulation for stress-strain distribution and microstructural evolution in 42CrMo steel during hot upsetting process," *Comp. Mater. Sci.*, **43**, 1117 – 1122 (2008).
21. Y. Lin and M. S. Chen, "Study of microstructural evolution during static recrystallization in a low alloy steel," *J. Mater. Sci.*, **44**, 835 – 842 (2009).
22. R. M. Su, Y. D. Qu, J. H. You, and R. D. Li, "Effect of pre-aging on stress corrosion cracking of spray-formed 7075 alloy in retrogression and re-aging," *J. Mater. Eng. Perform.*, **24**, 4328 – 4332 (2015).
23. B. Chen, W. M. Zhou, S. Li, et al., "Hot compression deformation behavior and processing maps of Mg – Gd – Y – Zr alloy," *J. Mater. Eng. Perform.*, **22**(9), 2458 – 2466 (2013).
24. V. I. Gorynin, S. Yu. Kondrat'ev, M. I. Olenin, and V. V. Rogozhkin, "A Concept of carbide design of steels with improved cold resistance," *Met. Sci. Heat Treat.*, **56**(9 – 10), 548 – 554 (2015).
25. H. E. Hu, X. Y. Wang, and L. Deng, "Comparative study of hot-processing maps for 6061 aluminium alloy constructed from power constitutive equation and hyperbolic sine constitutive equation," *J. Mater. Process. Tech.*, **30**(11), 1321 – 1327 (2014).
26. S. Wang, A. Nagao, P. Sofronis, and L. M. Robertson, "Hydrogen-modified dislocation structures in a cyclically deformed ferritic-pearlitic low carbon steel," *Acta Mater.*, **144**, 164 – 176 (2018).
27. W. J. Li, M. Y. Cai, D. Wang, et al., "Studying on tempering transformation and internal friction for low carbon bainitic steel," *Mater. Sci. Eng. A*, **679**, 410 – 416 (2017).
28. R. Feng, S. L. Li, Z. S. Li, and L. Tian, "Variations of microstructure and properties of 690 MPa grade low carbon bainitic steel after tempering," *Mater. Sci. Eng. A*, **558**, 205 – 210 (2012).
29. S. Sun, S. W. Yang, and G. L. Liu, "Evolution of microstructures of a low carbon bainitic steel held at high service temperature," *Acta Metall. Sin. (English Lett.)*, **27**, 436 – 443 (2014).